robotics

MDPI

Article

A Body Power Hydraulic Prosthetic Hand

Christopher Trent Neville-Dowler [1], Charlie Williams [1], Yuting Zhu [2,*] and Kean C. Aw [1]

[1] Department of Mechanical and Mechatronics Engineering, School of Engineering, University of Auckland, Auckland 1010, New Zealand; cnev969@aucklanduni.ac.nz (C.T.N.-D.); cwil659@aucklanduni.ac.nz (C.W.); k.aw@auckland.ac.nz (K.C.A.)
[2] School of Engineering, University of South Queensland, Springfield 4300, Australia
* Correspondence: yuting.zhu@unisq.edu.au

Abstract

Limb amputations are a growing global challenge. Electrically powered prosthetic hands are heavy, expensive, and battery dependent. Body-powered prostheses offer a simpler and lighter alternative; however, existing designs require high body forces to operate, exhibit poor aesthetics, and have limited dexterity. This study aims to present a design of a hydraulically actuated soft bending finger with a simple and scalable manufacturing process. This is then realised into a five-fingered body-powered prosthetic hand that is lightweight, comfortable, and representative of a human hand. The actuator was formed from two silicone materials of different stiffness (Stiff Smooth-Sil 950 and flexible Ecoflex 00-30) and reinforced with double-helix fibres to generate bending under internal hydraulic pressure. A shoulder-mounted hydraulic system has been designed to convert scapular elevation and protraction into actuator pressure. Finite element analysis and physical tests were performed to examine the bending and blocking force performance of the actuators. The physical actuators achieved bending angles up to 230 degrees at 60 kPa and blocking forces of 5.9 N at 100 kPa. The prosthetic system was able to grasp and hold a 320-g water bottle. The results demonstrate a soft actuator design that provides simple and scalable manufacturing and shows how these actuators can be incorporated into a body-powered prosthesis. This study provides a preliminary demonstration of the feasibility of human-powered prosthetics and necessitates continued research. This work makes progress towards an affordable and functional body-powered prosthetic hand that can improve the lives of transradial amputees.

Keywords: actuators; hydraulic pressure; body-powered prosthetic hand; soft robotics

Academic Editor: Xinjun Liu

Received: 10 December 2025
Revised: 24 December 2025
Accepted: 26 December 2025
Published: 4 January 2026

1. Introduction

Upper-limb loss imposes profound physical, functional, and psychosocial burdens on individuals with transradial amputations [1,2]. Though less common than lower-limb loss, it drastically affects daily life, with one-third of patients changing occupations and over half abandoning hobbies [3]. Major extremity amputations are projected to double by 2050, driven by aging populations and chronic disease, highlighting a growing need for effective interventions [4]. Despite technological advances, prosthetic rejection rates exceed 40% [5], largely due to discomfort, limited function, weight, maintenance, and poor aesthetics [6]. This underscores the urgent demand for prosthetic solutions that integrate functionality, usability, and anatomical realism. Limb amputations are prevalent worldwide, as is the demand for prostheses that meet user needs. Current prostheses available on the market

often do not meet the needs of the users. An affordable, comfortable, and lightweight prosthesis that functions well in diverse activities of daily living is needed.

Upper-limb prostheses can be separated into four broad categories: Passive, body-powered, myoelectric, and activity specific [3]. Each category comes with strengths and weaknesses, which makes suitability dependent on the use case. Having a broad range of prostheses in the market is useful, given there is significant variation in the priorities and preferences among prosthetic users [7]. According to the review by W. Xu et al. [3], passive prostheses include static devices that primarily serve a cosmetic purpose but can also assist in stabilising objects; Passive positional prostheses are also available with components that can be manually positioned; Activity-specific prostheses have limited capability because they are designed to perform a single, specific task, such as operating particular tools or sports equipment. The remaining types of prostheses, body-powered and myoelectric, are the most commonly prescribed [8]. Body-powered prostheses are powered by the user's own body, where movement of proximal body regions is leveraged to create distal movement in the prosthesis; Myoelectric devices are powered externally and are controlled by detecting electrical signals from the residual limb using electrodes [8].

Body-powered prosthetic hands remain a practical option for many users due to their mechanical simplicity, robustness, low cost, and the provision of natural proprioceptive feedback through direct coupling between body motion and device actuation [9]. However, conventional body-powered terminal devices typically rely on Bowden cable transmissions [10,11], which demand high input forces, limit grip patterns, and result in motion that often feels unintuitive or fatiguing to users [12]. Complex rigid-link designs can also reduce comfort and increase overall device mass [13].

2. Related Work

A body-powered prosthesis could offer a durable and lightweight solution that is not battery dependent; however, current designs are limited by the high force requirements and the limited degrees of freedom that are achievable. Previous attempts to solve the high force requirements have added excess weight or complexity to the prosthesis design, which prevents widespread adoption. Soft actuators offer a valuable opportunity to create compliant grippers capable of executing complex tasks with low weight and manufacturing costs. Elastomers with embedded fibres can be designed to bend with hydraulic actuation. Previous research [14] has demonstrated how this method can be applied in designing a prosthetic hand capable of grasping objects, which is body-powered with a wearable hydraulic actuating system. The current designs require complex manufacturing, which would prevent their widespread adoption in marketable prostheses. Therefore, creating a body-powered hydraulic soft actuator made from elastomeric materials that can be manufactured at a low cost of time and resources would be worthwhile. Furthermore, designing a wearable device to power the prosthetic will be necessary. This device will need to be comfortable and lightweight, which is a current challenge among body-powered wearable systems.

Recent developments in soft robotics offer an opportunity to address several of these limitations. Soft actuators made from elastomeric materials can provide compliance, adaptability, and lightweight construction, enabling grasping mechanisms that more closely resemble the motion of human digits [15,16]. Moreover, hydraulic soft actuators allow fine control of high forces with low input displacement, making them an attractive alternative to cable-based mechanisms for body-powered systems [17]. Soft fluidic actuators have shown improved safety, better conformity to objects during grasping, and simplified manufacturing compared to rigid-link prosthetic fingers [18,19].

Prosthetic fingers can improve the quality of life of amputees by providing a degree of hand function [17]. Prostheses have been a management tool for upper-limb amputees for decades. However, there is still a pressing need for improvements in the field of upper-limb prostheses, as they are often unaffordable or perform poorly in challenging environments [20]. A 2022 survey of 68 traumatic upper-limb amputees from Austria found that 44% of amputees abandoned their prosthesis [5]. The key reasons for abandonment in this study were comfort, weight, and function, which align with previous research [21]. The results showed that abandonment rates had not changed significantly since a 2007 study, which found mean abandonment rates of 45% and 35% for body-powered and electric prostheses, respectively [21]. Numerous recent developments in prosthetic hand technology have centred on electrically powered systems, utilising either pneumatic actuators or motor-driven mechanisms [22]. However, these devices are heavy, costly, and reliant on battery power. A further drawback of current body-powered prostheses is that they often come with limited degrees of freedom of movement [3]. Myoelectric prostheses can be designed with various terminal devices to achieve multiple degrees of freedom, enabling them to produce complex grip patterns [23]. Even so, with this benefit comes the drawbacks of myoelectric devices, including high cost, the requirement for batteries, increased weight, and complexity in fitting and repairing the devices [24]. Currently, users must choose between a more expensive and complex myoelectric device that offers greater degrees of movement freedom or a simple, lightweight, and robust body-powered device that requires higher forces to operate.

Body-powered devices are lightweight and remove the need for a battery source; however, they are not aesthetically appealing, have limited grip patterns, and can require high forces to operate [25]. Thus, there is a need for a functional body-powered prosthesis that reflects the appearance of a human hand and is easy to operate. This would reduce the likelihood of abandonment and assist upper-limb amputees in daily living.

By integrating soft robotics principles with practical prosthetic design constraints, this study contributes toward creating a functional, lower-cost, and anatomically representative body-powered prosthetic hand suitable for future clinical testing and user trials.

3. Concepts

3.1. Bending Actuator

The concept for the prosthetic hand system was to develop five finger-like bending actuators, contained within a holder representative of a human palm. The approach was to design finger actuators that bend when exposed to internal water pressure. Such an approach can be incorporated into a body-powered prosthetic system. By mounting a syringe between the waist and shoulder of a user, motion at their scapula can be utilised to compress the syringe and increase pressure inside the hydraulic lines. This concept utilises water pressure inside a hydraulic line, as it is less compressible than air and poses no concern regarding human exposure, unlike hydraulic oils.

A common method for inducing bending in soft actuators is to create different stiffness properties on opposite sides of the actuator. This approach has been used successfully in previous research by incorporating strain-limiting layers on one side [26] or varying fibre angles on opposite sides [27]. Internal pressurisation induces radial stress σ_r, circumferential stress σ_θ, and axial stress σ_z in the actuator, as shown in Figure 1. By incorporating radial reinforcement, the circumferential strain ϵ_θ can be restricted, which prevents the actuator from expanding radially. This modifies the stress state and increases axial elongation, evident by taking a linear small-strain approximation and applying Hooke's law, in Equation (1)

$$\epsilon_z = \frac{1}{E}(\sigma_z - v(\sigma_r + \sigma_\theta)) \quad (1)$$

where ϵ_z is axial strain, E is Young's Modulus, and ν is Poisson's ratio.

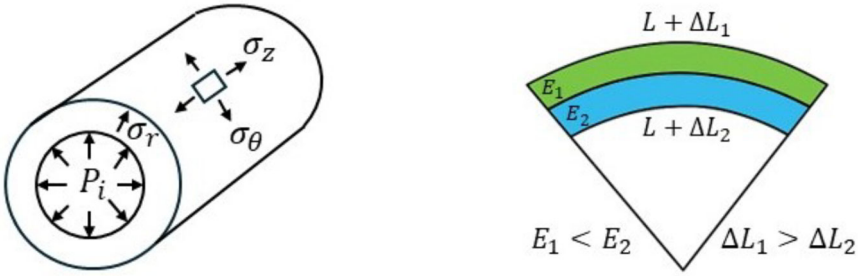

(**a**) (**b**)

Figure 1. Visual representation of the stress state and resultant bending in the finger actuators. (**a**) Stress state in the finger actuator; (**b**) Representation of how asymmetrical stiffness induces bending.

Restricting circumferential expansion alters σ_θ and σ_r so that the axial strain (elongation along the length of the actuator) increases. Equation (1) also shows that axial strain is inversely proportional to Young's modulus. If one side of an actuator has a lower modulus (stiffness) E, it will experience greater elongation than the stiff side, causing the actuator to bend towards the stiff side, as visualised in Figure 1. As shown in Figure 1a, the actuator is treated as a thick-walled cylinder; in Figure 1b, $E1$ is the Young's Modulus (stiffness) of material 1, $E2$ is the Young's Modulus (stiffness) of material 2, L is the starting length of both material sections, $\Delta L1$ is the change in length of material Section 1 (green), and $\Delta L2$ is the change in length of material Section 2 (blue). This concept of varying stiffness properties on either side of the actuator can be applied to create bending actuators for application in a hand prosthesis. Alternative approaches include modifying geometry to induce bending through asymmetric cross-sections [26] or internal cavities seen in PneuNet designs [28]; however, these come with added manufacturing complexity or unrealistic representations of the human finger.

The actuator was to induce bending by pressurising a flexible cylinder with different stiffnesses on each half and was expected to bend in the direction of the stiffer half, which would extend less than the flexible half. The benefit of this concept was inherent in its simplicity and the overall advantages of soft robotics for prosthetic applications. Additionally, this general concept has been proven to work in Kandasamy's work and others [14].

3.1.1. Finger Actuators Design

The actuator used was a thick-walled pressure vessel, capped at one end. The flexible thermoset polymer EcoFlex 00-30 (EF) formed the body of the actuator. Radial expansion was constrained by a double-helical wrapping of thread, approximately halfway through the thickness. Longitudinal expansion was constrained on one side by a 2 mm thick layer of Smooth-Sil 950 silicon (SS), while the other side of the actuator was entirely EF and free to extend. The end of the actuator was covered in a rounded cap of SS to prevent bulging. When pressurised using water, the combined effect was that the actuator bent in one direction, as the EF could extend further than the SS. It was then fitted to a hydraulic line.

A PC6 push-fit fitting was screwed into a 10 mm barbed fitting with anti-leak tape along the thread. This barbed fitting was then inserted into the open end of the actuator and secured with a rubber band. A 6 mm hydraulic line was then inserted into the PC6 connector, allowing the actuator to be pressurised without leaking. See Figure 2 for a labelled view of the actuator and fittings.

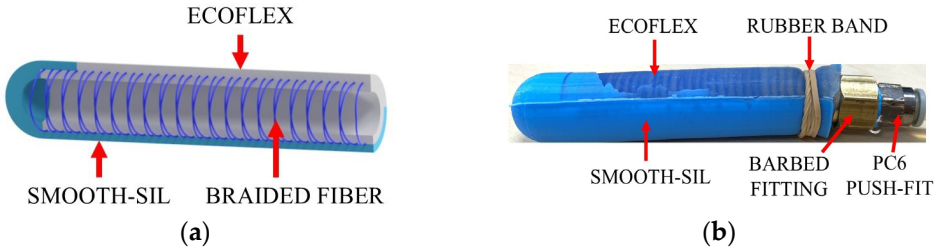

Figure 2. The finger actuator design: (**a**) Model of the finger actuator design; (**b**) Manufactured finger.

The bending actuator comprises two different hyperelastic silicone materials bonded to form a hollow cylindrical body. The two materials are Ecoflex 00-30 (EF30) and Smooth-Sil 950 (SS950), with SS950 being significantly stiffer. The inner half of the cylinder is purely EF30. Braided fibre (Kastking Braided Line 50 LB) is wound around this internal layer in a double-helix pattern, spanning the length of the actuator with a constant pitch of 2 mm. This braided line was used because it has been shown to successfully provide radial restraint in previous EF30 soft actuators [14]. Tests with nylon fishing line showed less effective bonding within silicone. A pitch of 2 mm was the highest pitch that prevented excessive radial bulging. The inner EF30 layer and fibre double helix are then enclosed by two distinct regions of EF30 and SS950, as shown in Figure 2a.

The arrangement of EF30 and SS950 allows the bottom half of the actuator to have greater stiffness than the top half. Having the stiffer SS950 wrapped around the tip prevents bulging at this location. When the internal pressure inside the actuator increases through compression of the syringe, the EF30 on the top half undergoes greater elongation than the SS950 on the bottom half, causing the actuator to bend towards the SS950 side. A circular cross-section is adopted to best represent human fingers, despite semi-circular cross-sections offering improved bending performance [26]. The manufactured finger is shown in Figure 2b.

3.1.2. Finger Actuator Manufacturing Process

Manufacturing the finger actuators requires a series of staged moulding processes, along with the winding of radially constraining fibres after the first moulding stage. The moulds used are displayed in Figure 3. These moulds were created using material extrusion 3D printing on a Bambu Lab A1 printer. Additive manufacturing is well-suited for designing moulds, as it allows for the formation of complex geometries with minimal time and cost, making it ideal for prototyping multiple mould and actuator designs.

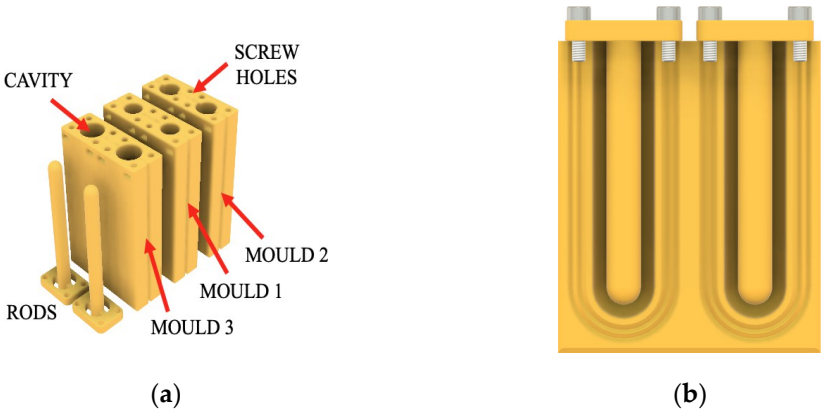

Figure 3. Moulds used for manufacturing the finger actuators: (**a**) Isometric view of the size set of the moulds and rods used to produce the actuator; (**b**) Open view of one half of the mould.

The actuator at each stage of the manufacturing process is displayed in Figure 4. For the first mould stage, EF30 is poured into the first mould, and then a rod is inserted to create an internal cylindrical cavity. Once cured, the rod, encased in a 2 mm layer of EF30, is removed from the mould. Braided fibres are then wrapped along the length of the EF30 layer in a double-helix pattern using a custom-designed automatic winding machine, shown in Figure 5. The rod is then inserted into the second mould, containing EF30, to form the EF30 layer on the top aspect of the cylinder. Once cured, the rod is removed and inserted into the third mould, containing SS950. This stage forms the SS950 surfaces that surround the bottom aspect of the cylinder and the distal tip. Once cured, the encased rod is removed from the mould and carefully retracted from the material, leaving the final formed actuator. At this stage, fittings are inserted into the open end and secured with a rubber band, as seen in Figure 2b.

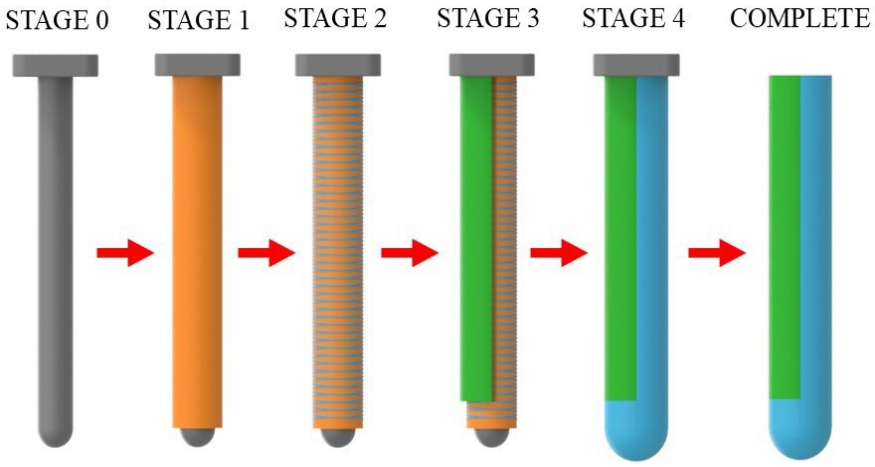

Figure 4. Stages of the manufacturing process for the finger actuators. Stage 0 is the rod before entering mould 1. Stage 1 is after the rod is removed from mould 1. Stage 2 follows the fibre-winding machine. Stage 3 is after the rod is removed from mould 2. Stage 4 is after the rod is removed from mould 3.

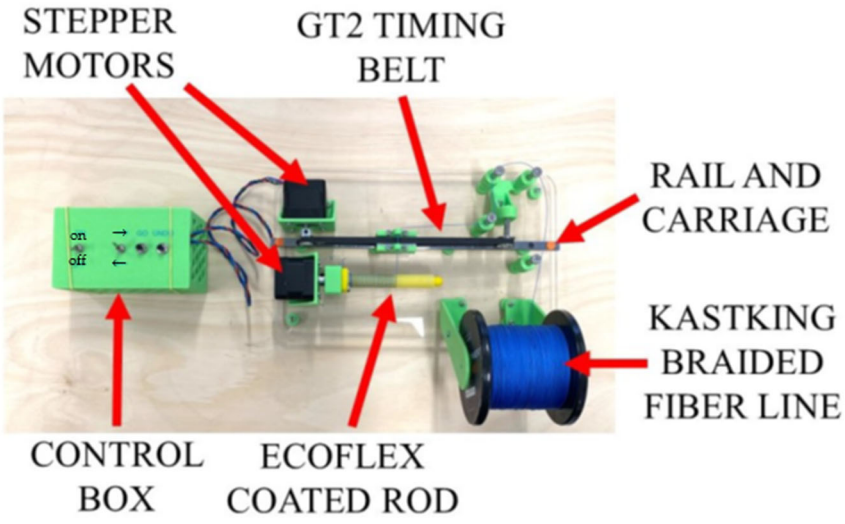

Figure 5. Top view of the automatic fibre winding machine for manufacturing the finger actuators.

The moulds were designed to allow the actuators to be removed easily without damage and prevent air bubbles from being trapped in the mould space. The mould contains a cylindrical cavity split along the longitudinal axis of the actuator, as shown in Figure 3b. This two-part design allows the mould to open, releasing the encased rod. At

each moulding stage, the rod is inserted after the liquid is poured in to prevent air bubbles from being trapped at the bottom of the cavity. The rod is secured with screws to ensure it aligns with the central axis of the mould.

Although the two-part mould allows easy removal, it brought the challenge of how to prevent excessive fluid leakage through the joint. Leakage causes the liquid level to drop, thus shortening the actuator length. Mould design and clamping strategies are implemented to overcome this issue. Initial testing was done using bolts to connect the two mould halves. This allows for a strong connection at the bolted joints; however, a less effective connection is maintained away from the bolt joints, which allows excessive leakage. The final design is clamped between two sheets of metal/acrylic using two G-clamps, providing a more distributed force over the mould area. Although it was noted that excessive clamping force causes the plastic moulds to gradually deform over repeated use. This is an unavoidable challenge with plastic moulds, which would be avoided with injection moulding tools for large-scale manufacturing. To further prevent leakage, sawtooth grooves were incorporated around the perimeter of the cavity space, as seen in Figure 3b. Impurities in the surface quality of the 3D printed moulds create gaps where liquid can pass through. The sawtooth groove allows a consistent connection between the two moulds.

3.2. Body-Powered Prosthetic Hand

Five bending actuators described above can be arranged into a hand and hence a prosthetic hand. As pressure is applied to all the fingers, they will bend. As the fingers are made from soft materials, they are naturally compliant, making them safe and not requiring sensing for force feedback.

3.2.1. Prosthetic System Design Mechanism

To power the prosthetic hand, a syringe enclosure was designed that adopts a drawbar spring mechanism. Figure 6b shows how tension in the strings at either end induces compression of the syringe. The enclosure was 3D printed to fit a 60 mL syringe. Figure 6a displays how this syringe enclosure is assembled. The syringe is mounted between the user's shoulder and hip, as displayed in Figure 7. As the user elevates and protracts their scapular, the syringe is compressed, increasing pressure inside the hydraulic line that connects to the finger actuators. As discussed previously, elbow extension or shoulder elevation and scapular protraction are common methods of generating body-power for a prosthetic hand. The current approach was preferred, as it does not restrict the user's elbow or arm motion when in use, allowing greater freedom of motion with the prosthesis. Furthermore, the syringe requires sufficient displacement to increase the water pressure inside five finger actuators. Utilising scapular elevation and protraction, rather than protraction alone, offers a greater range of motion. This approach has also been used previously [14] in a body-powered prosthetic hand, where the syringe was mounted between the shoulder and waist on an ipsilateral side. Testing the current design found that greater syringe compression could be achieved when the syringe was mounted on the opposite hip and shoulder, and the user both elevated and protracted their scapular compared to elevation alone.

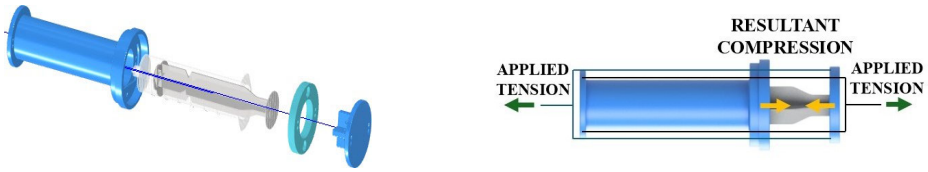

(**a**) (**b**)

Figure 6. Syringe assembly and mechanism of action: (**a**) Exploded view of the syringe assembly; (**b**) A drawbar-spring mechanism for the syringe.

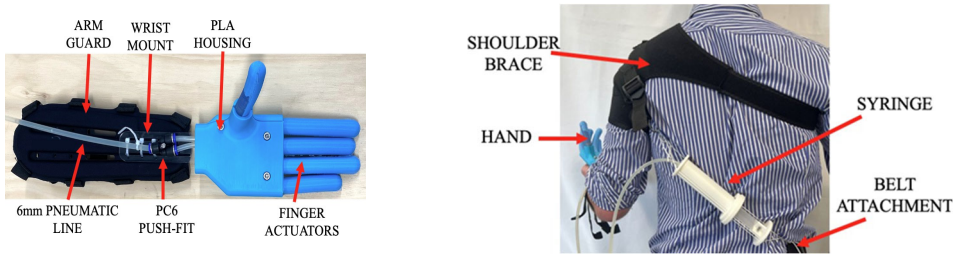

(**a**) (**b**)

Figure 7. Diagrams of the hand assembly and prosthetic: (**a**) Image of the finger holder and forearm attachment; (**b**) Prosthetic system components.

3.2.2. Finger Holder and Prosthetic System Design

The finger holder, shown in Figure 7a, is designed to constrain the fingers in an appropriate grasping orientation. The emphasis was placed on the orientation of the thumb to achieve an anthropomorphic appearance while maintaining gripping functionality. The finger holder is mounted to a wrist strap via an acrylic wrist mount, ensuring a secure attachment to the user's forearm. This approach allows non-amputees to test the system in a more realistic manner. A 6 mm pneumatic pipe is used as a hydraulic line to transfer water pressure from the syringe to the fingers. Push-fit connectors distribute a single hydraulic line to all five fingers. Barbed fittings, secured with rubber bands, are used to connect the pneumatic push-fit connectors to the finger actuators. This maintains a firm attachment under high internal pressures.

The current design shown in Figure 7 represents a more robust approach than the previous design [14]. The syringe enclosure prevents damage to the internal syringe, and a customised shoulder harness was designed to create a secure attachment to the user's shoulder. The opposite end of the syringe hooks onto a standard pants belt.

4. Modelling and Analysis

The model of finger actuator design was created and simulated using the finite element analysis (FEA) software Abaqus 2025. The FEA model conducted prior to manufacture allows for more rapid design iteration, which can closely resemble the actual actuator.

4.1. Model Setup

The FEA model replicates the geometry of the manufactured finger. Explicitly modelling the actuator increases the computation time of the model, which allows for understanding how each independent design component impacts the actuator's performance.

A hollow cylinder with a flat base cap and a rounded tip cap was created. A single actuator model was developed in Abaqus to closely replicate the actual actuator. A double-helical braided line was wrapped around the hollow tube with the rounded tip, which was assigned EF material properties. An additional EF-assigned layer covered one half, while the SS-assigned geometry covered the other half and the rounded tip region. Brass capped the actuator at the base, extending 15 mm into the cavity to represent the barbed fitting.

The double-helix fibres were secured to the cylinder's outer surface using a tie constraint, and the entire structure was enclosed by a larger cylinder and tip cap with a second tie constraint. The full model, highlighting the embedded fibres, is shown in Figure 8a.

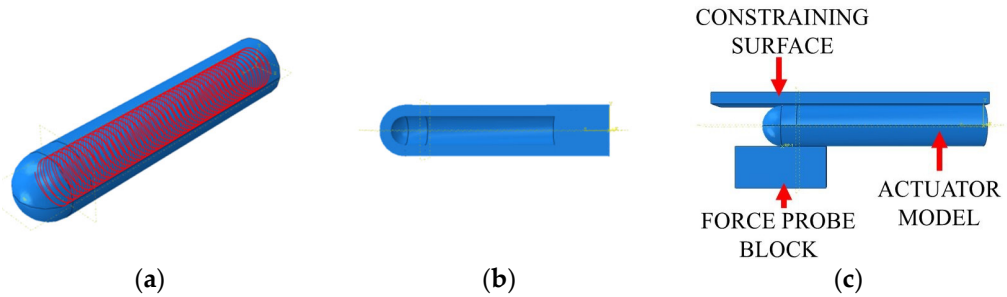

Figure 8. FEA model geometries for the bending angle and blocking force tests: (**a**) Finger actuator model with embedded fibres, the isometric view of the model showing the internal thread wrapping; (**b**) side section view of the model showing the internal cavity; (**c**) Blocking force setup.

Bending and blocking force tests were performed with the FEA model. For both cases, a zero-displacement boundary condition was applied to the flat end, where the hydraulic line inserts into the physical actuator. A pressure load was applied to the internal surface of the actuator. For the blocking test, a fixed probe block was positioned at the tip to block the motion of the actuator tip. Additionally, a constraining surface was aligned flush with the opposite side surface to maintain the actuator's horizontal position, as shown in Figure 8c. Surface-to-surface contacts were assigned between the actuator and the probe block, as well as between the actuator and the constraining surface. The blocking force was measured as the reaction force at a reference point tied to the probe block.

4.2. Material Properties

Three materials were used in the model. EF was characterised by a nonlinear hyperelastic third-order Ogden model, in accordance with the findings of Vishwakarma [29]. SS was characterised by a first-order Neo-Hooke hyperelastic model [19]. Finally, an isotropic linear elastic model with a Young's Modulus of 7.00 GPa and a Poisson's ratio of 0.36 was used for the KastKing thread. The Young's Modulus value was obtained from tensile testing by using a Universal Testing Machine in accordance with ASTM D3822 for the thread. The tensile test results are summarised in Table 1.

Table 1. Summary of the tensile test results from each KastKing thread sample and the average Young's Modulus used in the simulation.

Sample	Young's Modulus (GPa)
A	5.9228
B	7.801
C	6.8403
D	7.4371
Average	7.000

4.3. Simulation Convergence

Bending angle and blocking force tests were simulated on the model. In both tests, the model was constrained by applying a fixed support to the base of the actuator and through tie constraints between the bodies. Both tests investigated the effect of increasing the pressure force applied to the internal surface of the actuator model.

Separate meshes were generated for the helical wrapping and actuator body. For the actuator body, a 10-node quadratic tetrahedron element type (C3D10H) was used. For the

helical wrapping, a 3-node quadratic beam element (B32) was used as these elements more accurately capture curvature in thin geometries. This meshing approach was taken and justified in Wang, where an actuator with a similar geometry was modelled [27].

For both tests, mesh convergence was achieved at a 2 mm global seed size. There was a relatively small error between the 2 mm model and the finer 1.5 mm model (6.17% for the bending test and 3.17% for the blocking test). Additionally, for the finer 1.5 mm model, the simulated mesh could not be resolved past a 65 kPa pressurisation within the allowance time step of 1×10^{-5} for the bending test. Any minor improvement in accuracy from moving to the finer model would not justify the added computational time; therefore, the 2 mm global seed size was selected.

A convergence study was conducted by varying the global seed size of each actuator part. The bending and blocking force models were both converged at a global seed size of 2 mm. Refinement past this point brought issues with solver convergence. This is thought to be attributed to increased distortion of small elements when undergoing large deformations. These large deformations result in near-zero Jacobian determinants for some elements, indicating excessive element distortion. Thus, a 2 mm global seed was used for all analyses, which is in the range of those adopted in previous attempts to model soft fluidic actuators [10,26].

For each model, the global seed size was reduced from 6 mm to 1.5 mm to increase the total number of nodes. Tables 2 and 3 summarise the convergence results. The second finest mesh in each case corresponds to a global seed size of 2 mm. In both cases, the bending and blocking test results showed minimal deviation from the finest mesh size (1.5 mm), which supports that the model has converged.

Table 2. Summary of the bending angle convergence analysis and relative deviation between node densities.

Global Seed Size (mm)	6	4	2	1.5
Nodes	10,332	18,529	50,198	87,472
Bending angle (deg)	150.98	173.01	190.73	203.28
Deviation from fine mesh	25.73%	14.89%	6.17%	0%
Maximum pressure step (kPa)	70.6	80.9	88.1	65.2

Table 3. Summary of the blocking force convergence analysis and relative deviation between node densities.

Global Seed Size (mm)	4	2.5	2	1.5
Nodes	20,150	34,186	55,835	103,462
Blocking force (N)	1.27	1.24	1.21	1.25
Deviation from fine mesh	1.45%	1.24%	3.17%	0%
Maximum pressure step (kPa)	48	70.9	100	64.1

For the bending angle test, increasing pressures were applied to the inner surface of the actuator until the model could no longer be resolved. The actuator model was unconstrained and allowed to bend freely. The bending angle was measured by drawing a vector between a point at the centre of the terminal face of the floating rounded end-cap and another, 5 mm away, at the other end of the end-cap. As the actuator deformed, comparing the direction of this vector against a horizontal line yielded a measure of bending angle. It was assumed that the end-cap did not deform. The bending simulation response between 0 kPa to 80 kPa is shown in Figure 9.

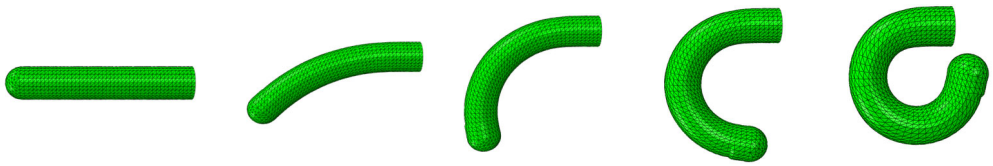

(**a**) 0 kPa (**b**) 20 kPa (**c**) 40 kPa (**d**) 60 kPa (**e**) 80 kPa

Figure 9. Soft actuator bending progression with applied internal pressures.

For the blocking force test, increasing pressures were applied to the inner surface of the actuator until the model could no longer be resolved. For this test, a cube model was created at the actuator tip using C3D20R elements, and a constraining flat plate was placed on the flexible (EF) side of the actuator using C3D8R elements. Both bodies were assigned steel material, with a Young's modulus of 215 GPa and a Poisson's ratio of 0.3. Surface-to-surface contacts were applied between these bodies and the actuator. A hard contact was assigned, with linear stiffness behaviour and a coefficient of friction of 1. This was informed by Berthold et al. [30]. As the internal pressure increased, the simulation measured the reaction force between the actuator tip and the contact nodes in the block. The images of simulations of the blocking force model at minimum and maximum internal pressures are shown in Figure 10.

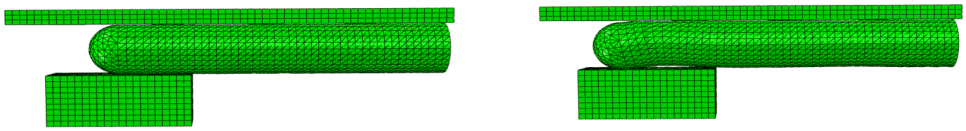

(**a**) 0 kPa (**b**) 78 kPa

Figure 10. Examples of soft actuator blocking force simulated at the 0 kPa and 78 kPa internal pressures.

4.4. Parametric Study Results

A parametric study was conducted to investigate the impact of actuator length, internal diameter, and wall thickness on the bending and force generation capabilities of the actuators. This is useful for informing the design of prosthetic hand fingers and for soft, fluidic actuators in broader applications. The parametric study plots are provided in Figure 11. The results show that for a given internal pressure, the bending angle increases with increasing actuator length, increasing internal diameter, and decreasing wall thickness. The blocking force was shown to increase with increasing wall thickness and internal diameter but remained constant with changes in actuator length.

Although longer and wider diameter fingers would generate greater bending and force output, this adds weight, increases the syringe displacements needed for actuation, and harms the anthropomorphic appearance of the fingers. Thus, prioritisation was given to designing fingers with an approximate length and diameter similar to those of human fingers. A 4 mm wall thickness was used for the fingers to achieve a high bending response.

The FEA simulation results in slight actuator curvature, which is excluded from the analytical calculation. Similarly, this analytical calculation assumes a constant cross-section, whereas the FEA simulation displays some circumferential strain, which would increase the area integral and force generated. Nevertheless, this calculation provides a reasonable order of magnitude estimate that aligns with the values calculated in the FEA simulation.

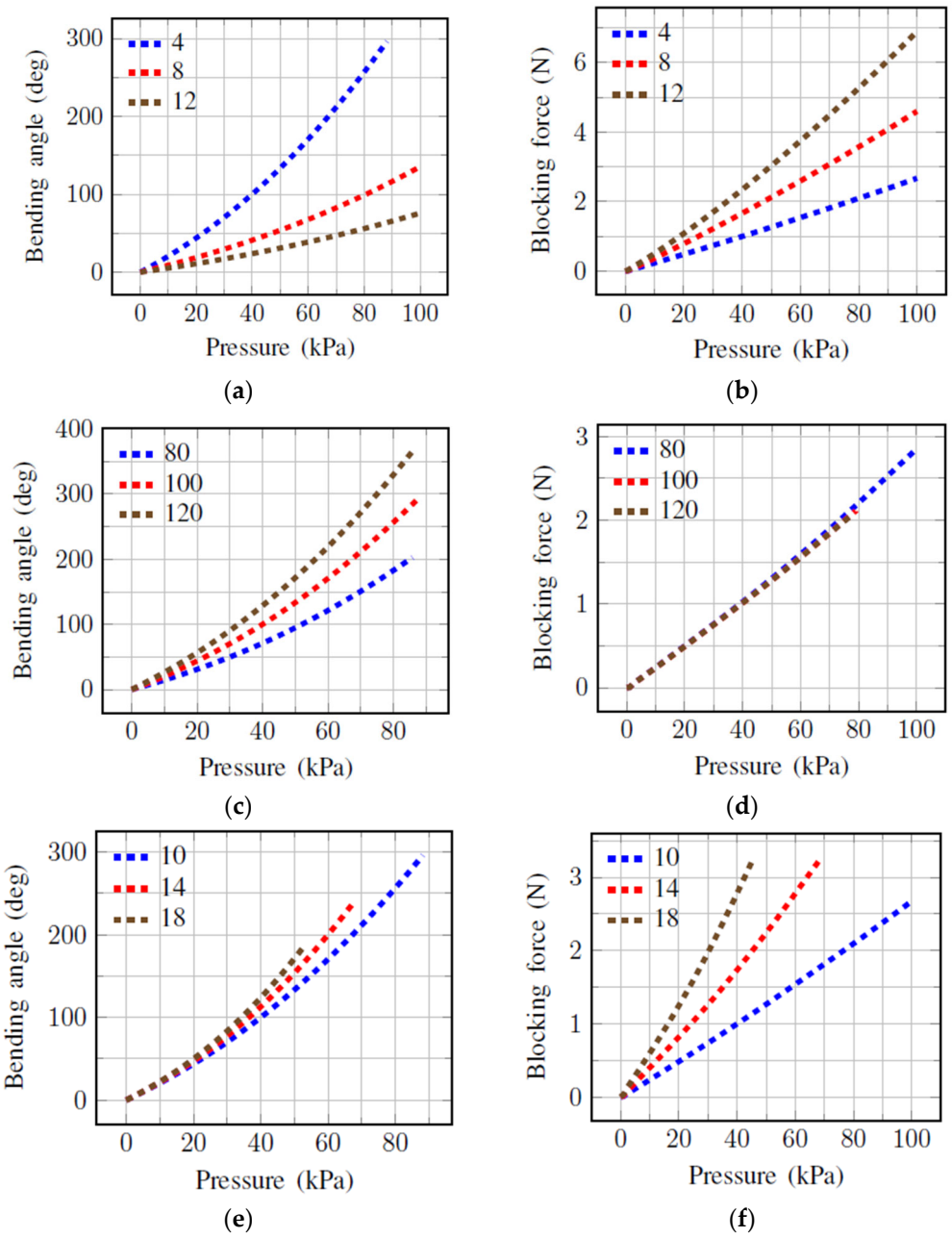

Figure 11. Parametric study results. Tested geometries are given in mm. (**a**) Bending angle vs. pressure at varying thickness; (**b**) Blocking force vs. pressure at varying thickness; (**c**) Bending angle vs. pressure at varying length; (**d**) Blocking force vs. pressure at varying length; (**e**) Bending angle vs. pressure at varying internal diameter; (**f**) Blocking force vs. pressure at varying internal diameter.

5. Experimental Evaluation

This section presents the physical testing and evaluates the results.

5.1. Finger Actuator Test Setup

Experiments were performed to determine the bending response and force generation when the fingers are internally pressurised. The full test procedure for the bending angle and blocking force tests is provided in Figure 12. For the bending test, the finger is free to rotate upwards as observed in Figure 12a. Bending in the horizontal plane would avoid gravity acting against the bending motion; however, the actuator sags downwards when held horizontal, which would begin the test with a negative bending angle. Thus, both tests were performed in the vertical plane.

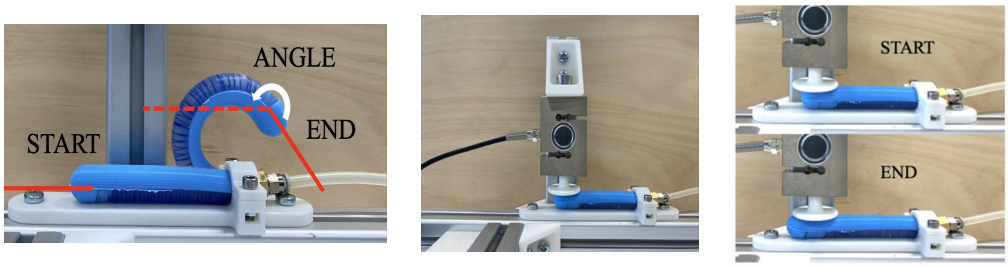

Figure 12. Side views of the bending angle and blocking force test setups: (**a**) Bending test setup and angle measurement; (**b**) Blocking force test setup for the actuator; (**c**) Start and end positions of the blocking test for the 100 mm actuator.

For the blocking test, the finger actuator is constrained in a horizontal position flush against a load cell sensor (QL Sensor GB/T 7551-2008) as seen in Figure 12b. When using hyperelastic materials, the force generation decreases as the bending angle increases [26]. Therefore, this test measures the maximum force generation capacity of the actuator at a given internal pressure level.

For both tests, a lead screw is rotated to compress the syringe and increase the water pressure inside the finger actuators, measured with a pressure gauge. For the bending test, pressure was increased in 10 kPa increments, and a photo was taken 25 cm from the actuator, which was used to determine the bending angle. The bending angle was calculated as the angle between a line normal to the actuator tip and the line of zero bending, as displayed in Figure 12a. For the blocking test, pressure was increased in 20 kPa increments. At each pressure value, the force measured on the load sensor was recorded. For the 100 mm actuator, each test was repeated three times on the same sample to identify any variations in the bending or pressure responses over time. The start and end positions of the blocking tests for the 100 mm actuator are shown in Figure 12. As the actuator is pressurised, the length increases as the restraining surfaces prevent any bending motion. The overall physical testing setup for the finger actuators is provided in Figure 13. The position of the 100 mm actuator at each pressure increment during the bending test is shown in Figure 14.

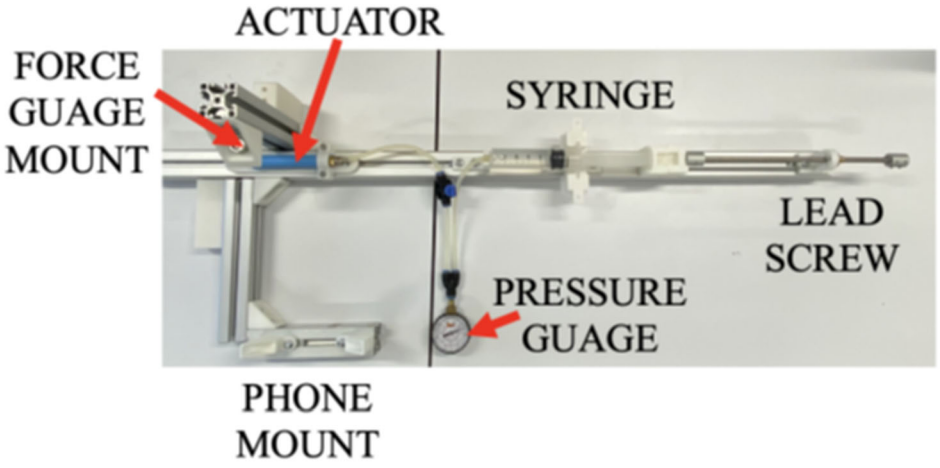

Figure 13. Physical testing setup—labelled wide view.

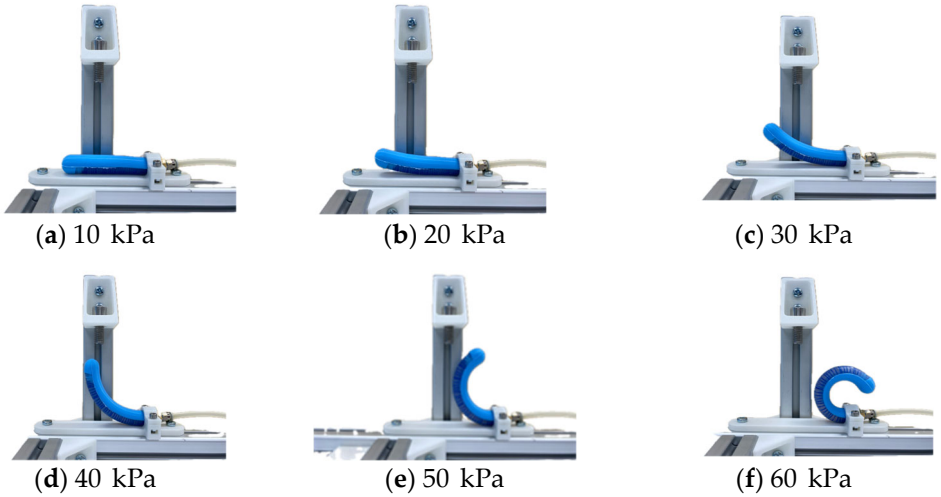

Figure 14. Bending of the 100 mm actuator observed at each pressure increment during the bending angle test.

The bending and blocking test results are shown in Figures 15 and 16, alongside the FEA results for comparison. The bending test data shows the same trend evident in the FEA results, whereas internal pressure increases, the bending angle increases nonlinearly. At low pressures, the physical testing showed significantly less bending angle compared to the FEA results at any given pressure, but the bending angle increased more rapidly with increasing pressure.

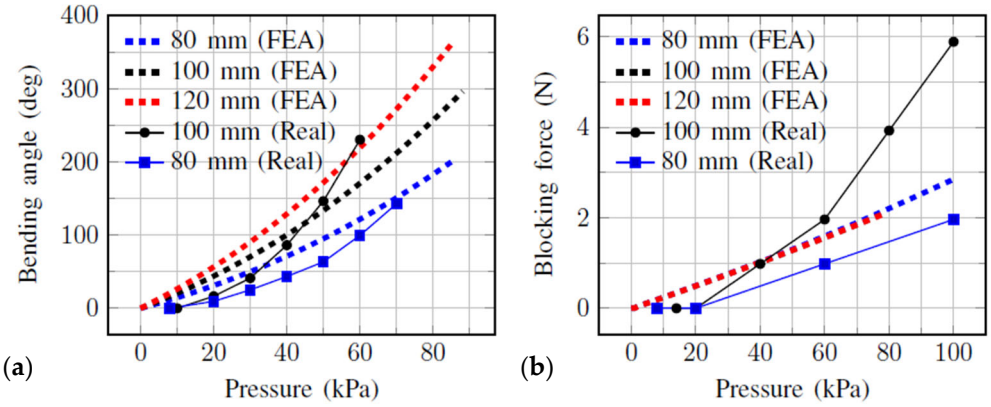

Figure 15. Physical experiment results compared against FEA results (**a**) Bending angle vs. pressure at varying length; (**b**) Blocking force vs. pressure at varying length.

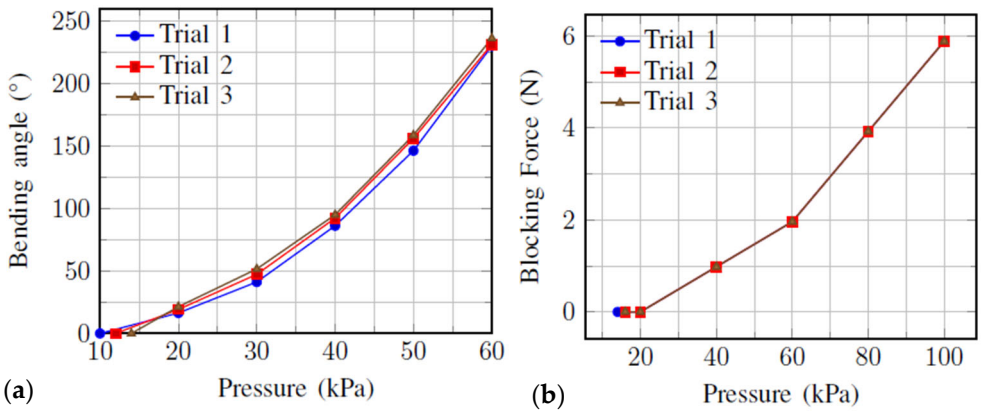

Figure 16. Repeated bending and blocking tests for the 100 mm physical actuator (**a**) Repeated bending angle tests (100 mm actuator); (**b**) Repeated blocking force tests (100 mm actuator).

Blocking force was constant with changing actuator length for the FEA results; however, the physical tests showed a higher blocking force at a given pressure for the 100 mm actuator compared to the 80 mm actuator. Overall, the FEA results over-predicted the 80 mm blocking force and under-predicted the 100 mm blocking force.

Repeated tests on the same 100 mm actuator sample revealed that the bending angle increased slightly with each test for a given internal pressure, while the blocking force remained constant.

5.2. Prosthetic System Testing

After designing and testing the finger actuators, the complete system was assembled and tested to demonstrate the full functionality of the prosthetic system. Figure 17a,b show the test subject wearing the prosthetic system and performing full actuation. The resulting scapular and hand positions are observable. The grasping capability of the system was tested by having the user attempt to grasp and hold a water bottle, as seen in Figure 17c. Once held, water was gradually added to the bottle until the bottle began to slip from the hand, after which the bottle was weighed. The test showed that a total weight of 322 g could be held before slip occurred.

(**a**) (**b**) (**c**)

Figure 17. Testing of the prosthetic hand system for grasping a water bottle: (**a**) Scapular position at full actuation (**b**) Hand position at full actuation (**c**) Water bottle held during the prosthetic system test.

6. Discussion

From design and simulation to manufacturing and physical testing, this study has developed and evaluated a prosthetic system.

6.1. Comparison of FEA and Physical Test Results

The results showed differences between the physical actuator testing and the FEA models, both in bending angle and blocking force. This can be explained by the FEA simulation being an ideal representation of the actuator. The tie constraints used assume perfect bonding between the silicone matrix and fibres. In reality, a perfect bond is not achieved, which means when the fingers are pressurised, the fibres can slip relative to the matrix. Figure 18 displays an actuator that was dissected after being exposed to large internal pressures, showing noticeable fibre shifting. Fras [31] states that fibre-reinforced actuators with larger fibre spacing show increased bulging, leading to greater degrees of bending and nonlinearity in response. Fibre shifting emulates a design with larger fibre spacing, which explains the greater bending nonlinearity relative to the FEA model.

(**a**) (**b**)

Figure 18. Evidence of bulging and resultant fibre shifting in the finger actuators; (**a**) Bulging of the finger actuator under high internal pressurisation; (**b**) Dissected finger actuator following high internal pressurisation.

This issue was a result of the way the thread was bonded within the actuator. EF, a silicon-based polymer [32], has a non-polar surface and, therefore, is resistant to chemical bonding to other materials. Hence, the thread was held in place solely through physical bonding. A lack of chemical bonding made the thread highly separable from the EF material surroundings, allowing bulges to form. A thread capable of being chemically bonded to the polymer, or a silicone glue between the thread and polymer, would be required to mitigate this failure mode. Alternatively, the fibre pitch could be optimised to further reduce the chance of bulging.

The manufacturing process employed in this study significantly advances upon previous research. Previous actuator designs have required manual labour to be produced. For example, for Kandasamy's actuator [14], manual insertion of pins into the actuator and winding the thread around these pins at varying angles on each side is laborious. For this design, thread winding is performed automatically to a set and consistent pitch using the winding machine. Other actuators have required manual intervention to apply a strain-limiting layer, such as a woven fabric, to one side of the actuator [26]. This need has been eliminated through the use of an additional moulding step, which applies a stiffer polymer (SS) to one side of the actuator.

Furthermore, the findings that the degree of bending angle under pressure slightly increased with repeated tests can also be explained by the fibre shifting. When the fingers are first pressurised to high values, initial slip of the fibres would occur. The slipped position of these fibres would remain once the pressure is relieved, which would increase the spacing and thus increase the bending response when the finger is re-pressurised. Nevertheless, the degree of change between tests is relatively small. The finding that blocking force remained unchanged despite the bending angle changing is likely because the effective change in force was less than the force sensor resolution.

Similarly, with longer actuator lengths, the area of material for bulging will increase, alongside the likelihood of manufacturing inconsistencies. Bulging would induce a larger cross-sectional area and length over which internal pressure is integrated, resulting in a greater blocking force. The FEA model under-predicts this due to the ideal conditions, which may explain the constant blocking force with increasing actuator length, unlike the physical testing.

6.2. Finger Actuator Performance

The physical testing shows a higher bending angle and blocking force response for a given internal pressure compared to similar fibre-reinforced actuators in the literature [14,27,33]. High bending angles and force output for given internal pressures are desirable characteristics in body-powered prostheses. High force requirements to operate a

prosthesis can cause pain and fatigue for the user [34] as well as reduce the ability to perceive and control their prosthesis [35]. Kandasamy et al. [14] designed a bending actuator also made of EF30, which required 50 kPa of internal pressure to achieve 50 degrees of bending, and 76 kPa generated 0.799 N of blocking force. This design induced asymmetric stiffness through different fibre braid angles on opposite sides of the actuator. Polygerinos et al. [26] presented a pneumatic Kevlar fibre-reinforced actuator made of EF30 with a fibreglass strain-limiting layer. The 130 mm long actuator achieved 250 degrees of bending at 205 kPa and 4 N of force at 100 kPa. In comparison, the current 100 mm actuator generates a greater bending and blocking force at a given internal pressure, with a 230-degree bending angle at 60 kPa and a 5.9 N blocking force at 100 kPa. Thus, inducing asymmetric stiffness through different silicone materials appears to allow for a greater bending angle and force generation at a given internal pressure compared to using different fibre braid angles or strain-limiting fabrics.

Although the current design has been used as a proxy for modelling an actuator with a strain-limiting layer [26,27], there does not appear to be any similar designs that have been manufactured and tested in the literature. Furthermore, this is the first instance found where this actuator design has been incorporated into a body-powered, five-fingered prosthetic hand. One of the main issues with the current design is the fibre shifting that has been discussed. This would lead to unpredictable behaviour and risks of failure over the long term. Therefore, strategies to prevent fibre shifting need to be implemented for this design to be adopted into a marketable body-powered prosthetic hand.

6.3. Performance of the Prosthetic Hand System

The testing of the prosthetic system demonstrated that the prosthesis could be used successfully to grasp a simple object, such as a water bottle. The actuation method of scapular elevation and protraction was able to generate sufficient force and syringe displacement to bend the fingers. These findings, alongside those from [33], display how a syringe mounted between the shoulder and waist can be used to actuate body-powered transradial prosthetic hands. Given the proportion of literature and consumer products [36] for body-powered transradial prosthetic hands are powered by motion at the elbow or protraction of the scapula through a chest strap, the current design presents a viable alternative.

The hand was able to grasp a 320-g water bottle before slip slipped, which fell short of the objective of 500 g, based on the weight achieved by [33]. Increasing the friction between the fingers and the object being grasped could increase the weight of the object. Kandasamy et al. [14] was able to hold a 500-g water bottle in their two-finger prosthesis; however, this test was performed with longer fingers that hooked underneath the water bottle rather than grasping the object from the side. Similarly, a recent three-fingered prosthetic hand design [37] was shown to generate 14.6 N of gripping force. This design used fibre-reinforced actuators with a strain-limiting layer to induce asymmetrical stiffness, similar to [34]. However, the objects that the hand was shown to grasp were small and held using a hooking motion from above. It is expected that the design presented in this paper would be capable of holding much heavier weights with the fingers hooked underneath, although human grasping motions are diverse and daily activities often require grasping objects from the side. The current design demonstrates the viability of a body-powered prosthesis with fluidic, elastomeric actuator fingers, capable of performing these grasping motions.

It is essential to note that the forces generated by the current prosthesis are significantly lower than those produced by the human hand. Ref. [38] found that the average gripping forces for adult populations range between 100 N and 500 N, depending on age and gender. The 320-g water bottle in the current test would equate to 3.1 N of weight force. This grasping capacity is significantly less than that of myoelectric prosthetic hand designs,

which can achieve over 100 N of gripping force. While even simple cable-actuated body-powered prostheses, such as the Hosmer hook, have demonstrated gripping forces of 33 N [39]. Evidently, the current design is a long way from being able to compete with the force generation capacity of these alternative prostheses. Nevertheless, the added gripping force in these designs comes with drawbacks. Myoelectric devices are heavier and battery-dependent, while the Hosmer hook only allows a rigid pinch mechanism, which limits the objects that can be held. With further development, the current design could have applications in tasks that require low forces, such as transporting light objects.

One aspect which limited the grasping ability in the current design was the lack of friction between the finger actuators and the water bottle. Initial testing of the system revealed very little friction between the silicone and plastic, making it challenging to grasp a water bottle from the side. Thus, tape was added to the surface of the water bottle to increase friction. Alternative approaches could include applying a rough surface to the actuator itself post-manufacture or incorporating a rough surface into the moulding process. Regardless, strategies need to be implemented to improve the friction coefficient of the finger actuators to make them capable of grasping a range of objects.

It could also be observed from the test that the gripping ability of the hand is limited by the force generation at the thumb. Although finger arrangement allows for a human-like appearance, having one thumb oppose four fingers is not necessarily the most optimal finger orientation to maximise gripping force. As can be observed in Figure 17c, the palm has a passive role in the gripping action, making minimal contact. Increasing the curvature of the palm would help improve the contact region and support the thumb in grasping objects; however, this would reduce the human-like appearance of the hand at rest. The inclusion of an inflatable palm region could be explored to improve the grasping capability of the hand. Such designs have been explored previously. For example, [40] designed a pneumatically actuated palm for grasping applications. The added force and water displacement volume required to actuate the palm in a body-powered device should be explored.

6.4. Manufacturing

A major technical advancement of this work is the efficient manufacturing process it offers. The current design outlines a manufacturing process that requires minimal manual labour time and limited moulding steps. This is a significant improvement on previous fibre-reinforced actuator designs. For example, the actuators shown in [27,36,41,42] all require the application of a strain-limiting layer, which involves manual application and an added drying time of the adhesive. Furthermore, they require separate moulding stages for each end cap and adopt manual fibre winding. Designs that use alternate fibre braid angles to induce asymmetric stiffness [14,33], require significant manual labour to wind the fibres. These aspects limit the viability for large-scale manufacturing and commercialisation. The current design allows for three moulding stages that can be implemented in large batches, with the fibre winding process automated for fast and reproducible products. The distal end cap is sealed as part of the third moulding stage, and barbed fittings prevent the need for moulding a cap where the hydraulic line is inserted.

6.5. FEA Results and Limitations

The trends shown in the parametric study align with those shown in the previous literature [26,33]. The parametric study results can clearly display the influence of design changes. In the context of fibre-reinforced soft actuators, manufacturing and testing are time-intensive and costly tasks with the development of unique moulds and sourcing of materials. The current results demonstrate how an efficiently designed FEA model,

utilising Abaqus scripting, enables the execution of numerous simulations with varied model parameters. This parametric study could be extended to examine the effect of using different silicone materials with different properties.

There are several limitations to the FEA model, stemming from challenges that accompany modelling non-linear, large deformations and fibre materials. Although beam elements are well-suited for modelling fibres, they do introduce bending stiffness into the model, which is not present in reality. Previous attempts to model fibres have approached this issue by arbitrarily reducing the fibre cross-sectional diameter by a factor of 2 [34,43]; however, this approach assumes that all deviations between the FEA and physical tests are attributed to the beam element properties. Discussions around the non-ideal bulging observed in this model support that this is not the case. Thus, the fibre diameter was not scaled in the current model. Future modelling attempts could involve performing bending stiffness tests on unit cell samples to determine the fibre diameter required to match both the tensile and bending stiffness properties. Testing a unit sample will allow the results to be extended to different actuator lengths. Unfortunately, individual tests would be required for different unit cell geometries, thus limiting the practicality of using the model as an early design tool.

6.6. Limitations of the Prosthetic Hand Design

One notable limitation of the current work is the small sample size that was used for testing the fingers. A total of four finger actuators were tested, one of each length, for both bending and blocking tests. The goal of the testing was to show proof of concept; however, a larger sample size would be required to accurately determine the bending and blocking force characteristics. These tests should also be repeated over long durations, such as 500 repetitions, as carried out by [14], to understand the design durability.

There are also limitations with the blocking force tests that were conducted. The force generation of the actuators was only measured in a horizontal position. Previous studies and analytical calculations have shown that the blocking force for bending actuators made of hyperelastic materials decreases as the bending angle increases [26]. This test was suited for examining the force capacity of the current design in the early stages and was adopted for testing previous soft actuators [14,26,44] which allows meaningful comparisons. However, further tests would be required to understand how the blocking force of the actuator varies with bending angle. A further limitation is that the prosthetic system was only tested on one subject with a simple grasping motion. This is because ethics approval for testing on human subjects was only obtained for one participant. Further testing should seek to include a larger sample of human subjects of various ages, genders, and sizes. Ethical approval with informed consent would be required for conducting this testing. To understand the true functionality of the prosthetic device, functional assessment, performance testing, and user experience evaluations are required. Box and Block tests are commonly used as a measure of gross dexterity and manipulation, while questionnaires are often used for rating user satisfaction [45–47]. These would be suitable initial tests to conduct on the body-powered prosthetic hand presented in this work.

7. Conclusions

In conclusion, the current work aimed to design a body-powered prosthetic hand that overcomes the current limitations of transradial prostheses, which are often heavy, expensive, battery dependent, or require high forces for body-powered actuation. This report has presented the design of a finger actuator that bends under internal pressure application by utilising asymmetric stiffness properties. This preliminary study demonstrates the feasibility of using human power to actuate bending actuators; however, it is

limited to a single grasping mode, in which all five fingers bend synchronously. It does not support independent finger control or multiple grip patterns such as precision pinch or lateral grasp. Thus, further work on repeatability, reliability, manufacturability, and clinical validation is required before a final prototype can be realised.

The finger actuator demonstrated high bending and blocking force performance relative to previous fluidic elastomeric actuators and was successfully incorporated into a body-powered five-fingered prosthetic hand. An FEA model was developed to inform design iterations, and both the model and practical testing showed that the bending and force characteristics can be modified through geometric changes. An efficient and scalable manufacturing process was also outlined, improving its viability for large-scale production. This represents a significant advancement over previous soft actuators, which require complex and labour-intensive manufacturing processes.

A wearable body-powered hydraulic system was designed to leverage scapular movement to actuate the prosthetic hand, which could grasp and hold a 320 g water bottle. Although the 500 g target was not achieved, all other objectives were met, and the grasping capacity could be improved by incorporating more palm involvement. This work advances the development of an affordable and functional body-powered prosthetic hand that can improve the lives of transradial amputees.

Author Contributions: Conceptualization, C.T.N.-D., C.W. and K.C.A.; methodology, C.T.N.-D., C.W. and K.C.A.; software, C.T.N.-D.; validation, C.T.N.-D. and C.W.; formal analysis, C.T.N.-D.; investigation, C.W.; resources, K.C.A.; data curation, C.T.N.-D. and C.W.; writing-original draft preparation, Y.Z.; writing-review and editing, Y.Z.; visualization, Y.Z.; supervision, K.C.A.; project administration, K.C.A. All authors have read and agreed to the published version of the manuscript.

Funding: This research received no external funding.

Institutional Review Board Statement: Ethical approval for this study series was obtained from the University of Auckland Human Participant Ethics Committee (approval number UAHPEC23153).

Data Availability Statement: Data is contained within the article.

Acknowledgments: We acknowledge that generative artificial intelligence tools were used to assist in the editing of language and grammar in this manuscript. We reviewed and verified all content generated by the AI tools to ensure accuracy and integrity and accept full responsibility for the final version of the work. The research was conducted in accordance with local statutory requirements.

Conflicts of Interest: The authors declare no conflicts of interest.

Abbreviations

The following abbreviations are used in this manuscript:

EF	Ecoflex 00-30
FEA	Finite element analysis
ASTM	American Society for Testing and Materials

References

1. McDonald, C.L.; Westcott-Mccoy, S.; Weaver, M.R.; Haagsma, J.; Kartin, D. Global prevalence of traumatic non-fatal limb amputation. *Prosthet. Orthot. Int.* **2021**, *45*, 105–114. [CrossRef]
2. Wei, B.; Zhang, J.; Cheng, Y.; Wu, H. Global, regional and national burden of traumatic amputations from 1990 to 2021: A systematic analysis of the Global Burden of Disease study 2021. *Front. Public Health* **2025**, *13*, 1583523. [CrossRef]
3. Xu, W.; Toyoda, Y.; Lin, I.C. Upper Extremity Prosthetics: Current Options and Future Innovations. *J. Hand Surg.* **2023**, *48*, 1034–1044. [CrossRef]
4. Ziegler-Graham, K.; MacKenzie, E.J.; Ephraim, P.L.; Travison, T.G.; Brookmeyer, R. Estimating the Prevalence of Limb Loss in the United States: 2005 to 2050. *Arch. Phys. Med. Rehabil.* **2008**, *89*, 422–429. [CrossRef]

5. Salminger, S.; Stino, H.; Pichler, L.H.; Gstoettner, C.; Sturma, A.; Mayer, J.A.; Szivak, M.; Aszmann, O.C. Current rates of prosthetic usage in upper-limb amputees–have innovations had an impact on device acceptance? *Disabil. Rehabil.* **2022**, *44*, 3708–3713. [CrossRef]
6. Stephens-Fripp, B.; Jean Walker, M.; Goddard, E.; Alici, G. A survey on what Australians with upper limb difference want in a prosthesis: Justification for using soft robotics and additive manufacturing for customized prosthetic hands. *Disabil. Rehabil. Assist. Technol.* **2020**, *15*, 342–349. [CrossRef] [PubMed]
7. Rekant, J.; Fisher, L.E.; Boninger, M.L.; Gaunt, R.A.; Collinger, J.L. Amputee, clinician, and regulator perspectives on current and prospective upper extremity prosthetic technologies. *Assist. Technol.* **2023**, *35*, 258–270. [CrossRef]
8. Engdahl, S.M.; Gonzalez, M.A.; Lee, C.; Gates, D.H. Perspectives on the comparative benefits of body-powered and myoelectric upper limb prostheses. *J. Neuroeng. Rehabil.* **2024**, *21*, 138. [CrossRef] [PubMed]
9. Ogura, R.; Itami, T.; Yoneyama, J. A Prototype Body-powered Prosthetic Hand Using Self-weight for Upper Limb Amputees in Return to Work. In Proceedings of the 2023 IEEE 21st International Conference on Industrial Informatics (INDIN), Lemgo, Germany, 18–20 July 2023; Institute of Electrical and Electronics Engineers Inc.: New York, NY, USA, 2023. [CrossRef]
10. Seamone, W.; Hoshall, C.H.; Schmeisser, G. *Modular Externally-Powered System for Limb Prostheses*. Available online: https://secwww.jhuapl.edu/techdigest/content/techdigest/pdf/APL-V10-N03/APL-10-03-Seamone.pdf (accessed on 9 December 2025).
11. Huaroto, J.J.; Suárez, E.; Vela, E.A. Wearable mechatronic devices for upper-limb amputees. In *Control Theory in Biomedical Engineering: Applications in Physiology and Medical Robotics*; Elsevier: Amsterdam, The Netherlands, 2020; pp. 205–234. [CrossRef]
12. Lu, Y.; Aoustin, Y.; Nocito, P.; Mick, S.; Jarrasse, N. Design and Experimental Validation of a Controller for Bowden-Cable Actuators Subject to Friction Variation. *IEEE Robot. Autom. Lett.* **2025**, *10*, 9264–9271. [CrossRef]
13. Li, X.; Liu, J.; Li, W.; Huang, Y.; Zhan, G. Force Transmission Analysis and Optimization of Bowden Cable on Body in a Flexible Exoskeleton. *Appl. Bionics Biomech.* **2022**, *2022*, 5552166. [CrossRef] [PubMed]
14. Kandasamy, S.; Teo, M.; Ravichandran, N.; McDaid, A.; Jayaraman, K.; Aw, K. Body-Powered and Portable Soft Hydraulic Actuators as Prosthetic Hands. *Robotics* **2022**, *11*, 71. [CrossRef]
15. Perera, O.; Liyanapathirana, R.; Gargiulo, G.; Gunawardana, U. A Review of Soft Robotic Actuators and Their Applications in Bioengineering, with an Emphasis on HASEL Actuators' Future Potential. *Actuators* **2024**, *13*, 524. [CrossRef]
16. Ilami, M.; Bagheri, H.; Ahmed, R.; Skowronek, E.O.; Marvi, H. *Materials, Actuators, and Sensors for Soft Bioinspired Robots*; John Wiley and Sons Inc.: Hoboken, NJ, USA, 2021. [CrossRef]
17. Motaghedolhagh, K.; Shariati, A.; Homer-Vanniasinkam, S.; Wurdemann, H. Soft Wearable Body-Powered Hydraulic Actuation System for a Prosthetic Finger Design. *IEEE Trans. Biomed. Eng.* **2024**, *71*, 3543–3555. [CrossRef]
18. Li, M.; Pal, A.; Aghakhani, A.; Pena-Francesch, A.; Sitti, M. Soft actuators for real-world applications. *Nat. Rev. Mater.* **2022**, *7*, 235–249. [CrossRef] [PubMed]
19. Xavier, M.S.; Fleming, A.J.; Yong, Y.K. Finite Element Modeling of Soft Fluidic Actuators: Overview and Recent Developments. *Adv. Intell. Syst.* **2021**, *3*, 2000187. [CrossRef]
20. Nagaraja, V.H.; da Ponte Lopes, J.; Bergmann, J.H.M. Reimagining Prosthetic Control: A Novel Body-Powered Prosthetic System for Simultaneous Control and Actuation. *Prosthesis* **2022**, *4*, 394–413. [CrossRef]
21. Smail, L.C.; Neal, C.; Wilkins, C.; Packham, T.L. Comfort and function remain key factors in upper limb prosthetic abandonment: Findings of a scoping review. *Disabil. Rehabil. Assist. Technol.* **2021**, *16*, 821–830. [CrossRef]
22. Geethanjali, P. Myoelectric control of prosthetic hands: State-of-the-art review. *Med. Devices* **2016**, *9*, 247–255. [CrossRef]
23. Resnik, L.; Acluche, F.; Lieberman Klinger, S.; Borgia, M. Does the DEKA Arm substitute for or supplement conventional prostheses. *Prosthet. Orthot. Int.* **2018**, *42*, 534–543. [CrossRef]
24. Gu, G.; Zhang, N.; Chen, C.; Xu, H.; Zhu, X. Soft Robotics Enables Neuroprosthetic Hand Design. *ACS Nano* **2023**, *17*, 9661–9672. [CrossRef] [PubMed]
25. Paquette, R.; Hill, O.; Carey, S.L.; Wernke, M.; Lura, D.; Knight, A.; Kahle, J.T.; Miro, R.M.; Highsmith, M.J. Utility of Body-Powered Voluntary Opening and Closing Terminal Devices on Transradial Prostheses. *Technol. Innov.* **2025**, *24*, 46–57. [CrossRef]
26. Polygerinos, P.; Wang, Z.; Overvelde, J.T.B.; Galloway, K.C.; Wood, R.J.; Bertoldi, K.; Walsh, C.J. Modeling of Soft Fiber-Reinforced Bending Actuators. *IEEE Trans. Robot.* **2015**, *31*, 778–789. [CrossRef]
27. Wang, Z.; Polygerinos, P.; Overvelde, J.T.B.; Galloway, K.C.; Bertoldi, K.; Walsh, C.J. Interaction Forces of Soft Fiber Reinforced Bending Actuators. *IEEE/ASME Trans. Mechatron.* **2017**, *22*, 717–727. [CrossRef]
28. Rad, C.; Hancu, O.; Lapusan, C. Data-Driven Kinematic Model of PneuNets Bending Actuators for Soft Grasping Tasks. *Actuators* **2022**, *11*, 58. [CrossRef]
29. Vishwakarma, A.R. *A Method for Characterization of Soft Polymer*; [Order No. 30989041]; State University of New York at Buffalo: Buffalo, NY, USA, 2024.
30. Berthold, R.; Burgner-Kahrs, J.; Wangenheim, M.; Kahms, S. Investigating frictional contact behavior for soft material robot simulations. *Meccanica* **2023**, *58*, 2165–2176. [CrossRef]

31. Fras, J.; Althoefer, K. Soft Fiber-Reinforced Pneumatic Actuator Design and Fabrication: Towards Robust, Soft Robotic Systems. In *Towards Autonomous Robotic Systems*; Lecture Notes in Computer Science (Including Subseries Lecture Notes in Artificial Intelligence and Lecture Notes in Bioinformatics); Springer: Cham, Switzerland, 2019; pp. 103–114. [CrossRef]
32. Smooth-On. Available online: https://www.smooth-on.com/products/ecoflex-00-30/ (accessed on 8 December 2025).
33. Wang, B.; McDaid, A.; Giffney, T.; Biglari-Abhari, M.; Aw, K.C. Design, modelling and simulation of soft grippers using new bimorph pneumatic bending actuators. *Cogent Eng.* **2017**, *4*, 1285482. [CrossRef]
34. Biddiss, E.; Chau, T. Upper limb prosthesis use and abandonment: A survey of the last 25 years. *Prosthet. Orthot. Int.* **2007**, *31*, 236–257. [CrossRef] [PubMed]
35. Hichert, M.; Plettenburg, D.H. Ipsilateral Scapular Cutaneous Anchor System: An alternative for the harness in body-powered upper-limb prostheses. *Prosthet. Orthot. Int.* **2018**, *42*, 101–106. [CrossRef]
36. Dynamics, A. Introduction to Body-Powered Prostheses. Available online: https://www.armdynamics.com/upper-limb-library/introduction-to-body-powered-prostheses (accessed on 8 December 2025).
37. Zhang, N.; Ren, J.; Dong, Y.; Yang, X.; Bian, R.; Li, J.; Gu, G.; Zhu, X. Soft robotic hand with tactile palm-finger coordination. *Nat. Commun.* **2025**, *16*, 2395. [CrossRef]
38. Nilsen, T.; Hermann, M.; Eriksen, C.S.; Dagfinrud, H.; Mowinckel, P.; Kjeken, I. Grip force and pinch grip in an adult population: Reference values and factors associated with grip force. *Scand. J. Occup. Ther.* **2012**, *19*, 288–296. [CrossRef] [PubMed]
39. Smit, G.; Bongers, R.M.; Van der Sluis, C.K.; Plettenburg, D.H. Efficiency of voluntary opening hand and hook prosthetic devices: 24 years of development? *J. Rehabil. Res. Dev.* **2012**, *49*, 523–534. [CrossRef]
40. Deimel, R.; Brock, O. A novel type of compliant and underactuated robotic hand for dexterous grasping. *Int. J. Robot. Res.* **2016**, *35*, 161–185. [CrossRef]
41. Ye, Y.; Scharff, R.B.N.; Long, S.; Han, C.; Du, D. Modelling of soft fiber-reinforced bending actuators through transfer learning from a machine learning algorithm trained from FEM data. *Sens. Actuators A Phys.* **2024**, *368*, 115095. [CrossRef]
42. Rakhtala, S.M.; Ghayebi, R. Real time control and fabrication of a soft robotic glove by two parallel sensors with MBD approach. *Med. Eng. Phys.* **2022**, *100*, 103743. [CrossRef]
43. Decroly, G.; Mertens, B.; Lambert, P.; Delchambre, A. Design, characterization and optimization of a soft fluidic actuator for minimally invasive surgery. *Int. J. Comput. Assist. Radiol. Surg.* **2020**, *15*, 333–340. [CrossRef]
44. Wang, B.; Aw, K.C.; Biglari-Abhari, M.; McDaid, A. Design and fabrication of a fiber-reinforced pneumatic bending actuator. In Proceedings of the 2016 IEEE International Conference on Advanced Intelligent Mechatronics (AIM), Banff, AB, Canada, 12–15 July 2016; pp. 83–88. [CrossRef]
45. Susanto, N.; Prastawa, H.; Mahachandra, M.; Rakhmawati, D.A. Evaluation of Usability on Bionic Anthropomorphic (BIMO) Hand for Disability Hand Patient. *J. Ilm. Tek. Ind.* **2019**, *18*, 124–133. [CrossRef]
46. Haverkate, L.; Smit, G.; Plettenburg, D.H. Assessment of body-powered upper limb prostheses by able-bodied subjects, using the Box and Blocks Test and the Nine-Hole Peg Test. *Prosthet. Orthot. Int.* **2016**, *40*, 109–116. [CrossRef]
47. Kalita, A.J.; Chanu, M.P.; Kakoty, N.M.; Vinjamuri, R.K.; Borah, S. Functional evaluation of a real-time EMG controlled prosthetic hand. *Wearable Technol.* **2025**, *6*, e18. [CrossRef]